Ecological Modelling 247 (2012) 210–220

Contents lists available at SciVerse ScienceDirect

Ecological Modelling

journal homepage: www.elsevier.com/locate/ecolmodel

Bayesian hierarchical modeling of Pacific geoduck growth increment data and climate indices

Thomas E. Helser[a,*], Han-lin Lai[b], Bryan A. Black[c]

[a] Resource Ecology and Fisheries Management Division, Alaska Fisheries Science Center, National Marine Fisheries Service, National Oceanic and Atmospheric Administration, 7600 Sand Point Way, Seattle, WA 98115, USA
[b] Fisheries Statistics Division, F/ST1, Office of Science and Technology, National Marine Fisheries Service, National Oceanic and Atmospheric Administration, 1315 East West Highway, Silver Spring, MD 20901, USA
[c] Hatfield Marine Science Center, 2030 SE Marine Science Drive, Oregon State University, Newport, OR 97365, USA

ARTICLE INFO

Article history:
Received 24 March 2012
Received in revised form 22 August 2012
Accepted 30 August 2012
Available online 29 September 2012

Keywords:
Pacific geoduck
Growth increment
Pacific Decadal Oscillation
Climate change
Bayesian model
Hierarchical model
North Pacific Ocean

ABSTRACT

Growth increment widths from hard structures of marine and freshwater fish and bivalve species are increasingly used to model growth and elucidate relationships with environmental variability. Fully characterizing the intrinsic age-related growth variation among individuals within and between populations, while estimating the extrinsic environmental effects simultaneously, can be challenging. Using the long-lived bivalve Pacific geoduck (*Panopea generosa*), we develop an integrated approach to analyze the relationship between growth increment data and climate indices using Bayesian hierarchical methods. Fitting models to growth increment data from multiple individuals over two sites, we examined different covariance structures related to random individual effects, long- and short-term environmental effects and unexplained errors. The best fitting hierarchical model accounted for a site-specific mean growth response, individual growth variability through random parameter effects, and site-specific error variances. Extrinsic environmental effects on growth were also significant and included a random year effect and the Pacific Decadal Oscillation (PDO) as a predictor of mean growth across both individuals and sites. Once intrinsic age-related growth was accounted for, PDO accounted for 18% to total variability in growth increment data; geoduck shell size was predicted to increase as a function of larger PDO anomalies. However, the greatest variability in growth increment data was explained by random year effects (~60–70%), and while largely unexplained, sea surface temperature (SST) is a likely determinant on geoduck growth rates showing a positive growth–SST response.

Published by Elsevier B.V.

1. Introduction

The tendency for individuals from single or even multiple locations to exhibit synchronous growth patterns provides strong evidence that environmental processes can have a mechanistic influence on growth. For nearly a century, tree-ring science (dendrochronology) has been at the forefront of developing proxies for a range of climate and disturbance phenomena including temperature, precipitation, and river discharge as well as fires, insect outbreaks, and windstorms (Speer, 2010; Cook and Kairiukstis, 1990). Reconstructions often span several hundred years, and even millennia when chronologies developed from living trees are combined with dead-collected, preserved material (Ferguson, 1968; Eronen et al., 2002). In recent years, these methods have been adapted to biogenic calcified structures in marine organisms including coral (Correge, 2006), bivalves (Butler et al., 2009), and fish (Black et al., 2008a) for reconstructing past environmental variability in these aquatic environments. Morphological, chemical, and isotopic properties of annual growth increments formed in marine organismal hard structures capture a wide range of environmental variables including temperature, upwelling, growth, and, productivity, among others (i.e., Goman et al., 2008; Killingley and Berger, 1979; Krantz et al., 1987; Marchitto et al., 2000). Thus, growth increments can yield valuable information concerning the physical and biological processes that affect growth, and also serve as proxies to reconstruct climate and environmental records in these marine environments where observational records are relatively scarce.

Methods of analyzing growth increment data have varied, depending on the scientific discipline. In fisheries science, the focus was traditionally on back-calculation methods to derive a past measure of body size predicted from growth increments in fish scales and otoliths (Ricker, 1975), many of which involved regression analysis (Francis, 1990). More recently, attention has turned to teasing out environmental or physical effects suspected of influencing

* Corresponding author. Tel.: +1 206 526 4200; fax: +1 206 526 6723.
E-mail addresses: Thomas.helser@noaa.gov, thom_hoster@yahoo.com (T.E. Helser).

0304-3800/$ – see front matter. Published by Elsevier B.V.
http://dx.doi.org/10.1016/j.ecolmodel.2012.08.024

growth increment data during particular calendar years in addition to modeling age-related growth using analysis of variance (Hagen and Quinn, 1991; Weisberg, 1993) and mixed effects (Weisberg et al., 2010) models. Nevertheless, partitioning and estimating growth variation among intrinsic age- or size-related effects and extrinsic environmental effects, while fully characterizing growth variability within and between populations is an active area of research in fisheries and ecology.

In dendrochronology, growth increment data are analyzed through a process called detrending; each measurement time series is fit with a function that models age-related growth declines and divides each measurement by the predicted value, thereby removing the non-stationary tree aging process into relative ring-width indices of unit mean and a constant variance. The entire ensemble of detrended tree ring time series is then averaged to derive a common signal across the series for each calendar year and is referred to a chronology (Fritz, 1976). The quality of the chronology is ensured by crossdating which involves the matching of synchronous growth patterns induced by climate variability among all samples of a given species and site. In so doing, any missed or falsely added increments can be identified, guaranteeing annual resolution in the data. A limitation of most detrending techniques is that processes of greater duration than the measurement time series length cannot be resolved (Cook et al., 1995), though methods have evolved that better preserve low-frequency signals, especially when datasets contain live- and dead-collected material (Esper et al., 2002; Bunn et al., 2004). Nonetheless, techniques for detrending, averaging and chronology development remain controversial topics in modern dendrochronology.

In this paper, we developed an integrated approach to analyzing growth increment data in a marine paleoclimate time series using Bayesian hierarchical methods. This approach represents a more general statistical methodology for the analysis of growth increment data because it partitions and estimates both the intrinsic age and extrinsic climate effects on growth variability. We demonstrate this method using a data set of annual growth increment measurements in Pacific geoduck (*Panopea generosa*) samples collected near Vancouver Island from a study by Black et al. (2009). Geoduck can reach 150 years of age and have been studied as a proxy for reconstructing North Pacific sea surface temperatures (SST) (Strom et al., 2004). Our goal is not to dismiss other approaches used in the field of dendrochronology but rather to add another tool for analyzing the relationship between climate variability and growth in marine organisms.

Bayesian methods have often been used as the quantitative framework for employing meta-analysis, and numerous examples are available in the ecological (Wade, 2000; Helser and Lai, 2004) and fisheries science (Punt and Hilborn, 1997; Helser et al., 2007) literature. In recent years, Bayesian hierarchical models have been also applied to tree-ring time series (Boreux et al., 2009). Bayesian methods (Gelman et al., 2004) in particular provide a direct means of parameter estimation and quantification of uncertainty in variance components and model parameters, as well as functions of parameters. By taking advantage of nested data structure, we fit an allometric linear hierarchical growth function to detrend growth increment data from all individuals simultaneously over several sites from which geoduck were collected and test for different covariance structures among random individual effects, environmental effects and residual error. A particular strength of this approach is that statistical properties of the observations related to the chronology are well described. In addition, the approach provides a novel means by which to quantify uncertainty between growth–climate relationships. Specifically our goals were to: (i) construct a geoduck growth model that estimates climate–growth response and (ii) estimate the strength of the environmental effects by explicitly estimating the variance components and their appropriate variance structure within the model. Previous studies have implicated SSTs, especially at a local scale, and the Pacific Decadal Oscillation (PDO), especially at a basin-wide scale, as environmental factors affecting the growth response of animals in the North Pacific Ocean (Francis and Hare, 1994; Black et al., 2009). These climate indices were natural candidates for inclusion in the geoduck modeling framework presented in this paper.

2. Materials and methods

Pacific geoduck are a long-lived bivalves distributed from Kodiak, Alaska to southern California and are found in the seafloor sediment from the intertidal zone to depths of 100 m (Coan et al., 2000). Geoduck is a good candidate for examining environmental variability of growth and for historical climate reconstruction because they can live more than 150 years (Strom et al., 2004; Black et al., 2009) and occupy habitat in the mixed layer where they are responsive to environmental variability (Bernard, 1983). This study used Pacific geoduck that had been live-collected from two different sites: (1) Tree Nob, located along the northern coast of British Columbia and (2) Barkley Sound, located along the southwestern coast of Vancouver Island (Fig. 1). Tree Nob data are described in Black et al. (2008b) while the Barkley Sound data are newly developed. Crossdated chronologies were generated for each of the sites and crossdated estimates of total geoduck age were obtained for each individual (Fig. 1). For the analysis presented in this study, 33 individuals were measured at the Tree-Nob site, spanning nearly a century while 15 individuals were measured at Barkley Sound, spanning more than 70 years (Fig. 2). When sorted as a function of the age at which a particular growth increment was formed, both data sets exhibited the typical negative exponential decay beginning with relatively large increment widths at young ages followed by a continuous monotonic decline over subsequent ages (Fig. 2). This intrinsic growth pattern is typical of the allometric relationship between somatic body size and age in marine organisms.

2.1. Sample preparation and data development

In Pacific geoduck, the hinge plate (chondrophore) grows at a rate proportional to that of the outer shell layer, but is protected from erosion and thus provides the most complete growth record (Shaul and Goodwin, 1982). As such, shell preparations, growth increment counts and growth increment measurements were restricted to the hinge plate area, and followed the same general methods as reported by Black et al. (2009). A single sample from each geoduck specimen was cut on the dorso-ventral axis of the valve through the umbro and hinge plate using a diamond blade lapidary saw. The cut surface was polished with 600-grit sandpaper and then etched with 2% hydrochloric acid. An impression (acetate peel) was made by pressing the etched surface of the hinge plate against a piece of acetate film softened with a drop of acetone. The peel was sandwiched between two glass slides and viewed either by a microprojector or a dissecting microscope, both using transmitted light.

Only those peels with annual growth increments (bands) sufficiently clear that they could be measured were digitally photographed using a Leica DC300 3.2 megapixel camera interfaced with a Leica stereomicroscope. These samples were then visually crossdated to ensure that all increments were assigned the correct calendar year of formation. Crossdating assumes that some aspect of the environment limits growth and induces synchronous growth patterns among all individuals from a given site (Fritz, 1976; Stokes and Smiley, 1996). Fundamental in all tree-ring studies, crossdating is accomplished by matching this synchronous pattern among samples, beginning at the marginal increment formed at

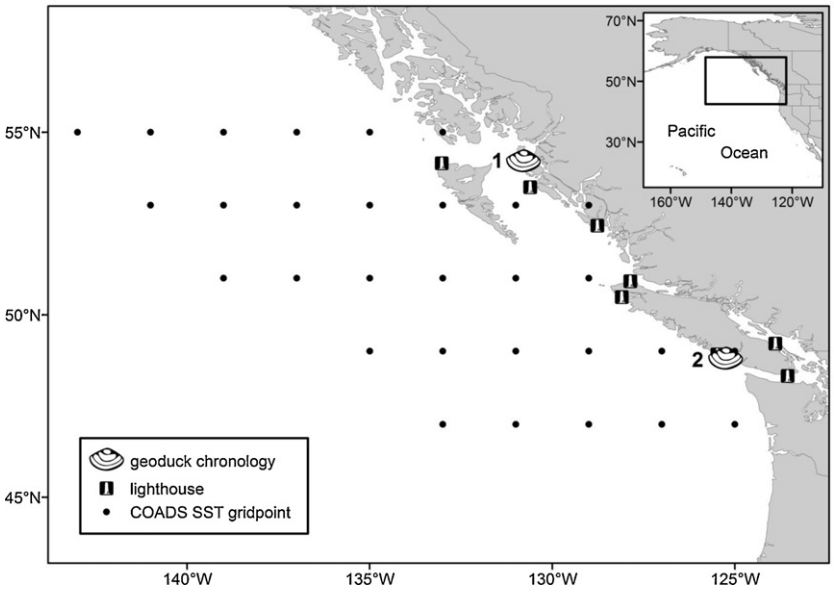

Fig. 1. Sampling sites of Pacific geoduck used in this study: (1) Tree Nob and (2) Barkley. Also shown are lighthouse stations and COADS grid points from which sea surface temperatures were obtained to derive regional sea surface temperatures (SST) and SST anomalies.

the known year of capture and working toward the center. If an increment is accidentally missed or falsely added, the growth pattern for that individual will be offset relative to that in the other samples, thereby identifying the error. Once crossdated, growth increment widths were measured along continuous transects that followed the axis of growth using Image Pro Plus 6.0. Each growth increment was delineated at the end of the winter line (translucent zone) and start of the new growing season (opaque zone) (Shaul and Goodwin, 1982).

To statistically verify the visual crossdating, measurement time series were imported into the International Tree-Ring Data Bank Dendrochronology Program Library program COFECHA written in 1982 by Richard Holmes of the Laboratory of Tree-Ring research at the University of Arizona (available through the University of Arizona Laboratory of Tree-Ring Research Web site: www.ltrr.arizona.edu/software.html). COFECHA removes low-frequency variability from each measurement time series, thereby isolating high-frequency, year-to-year growth patterns. Each

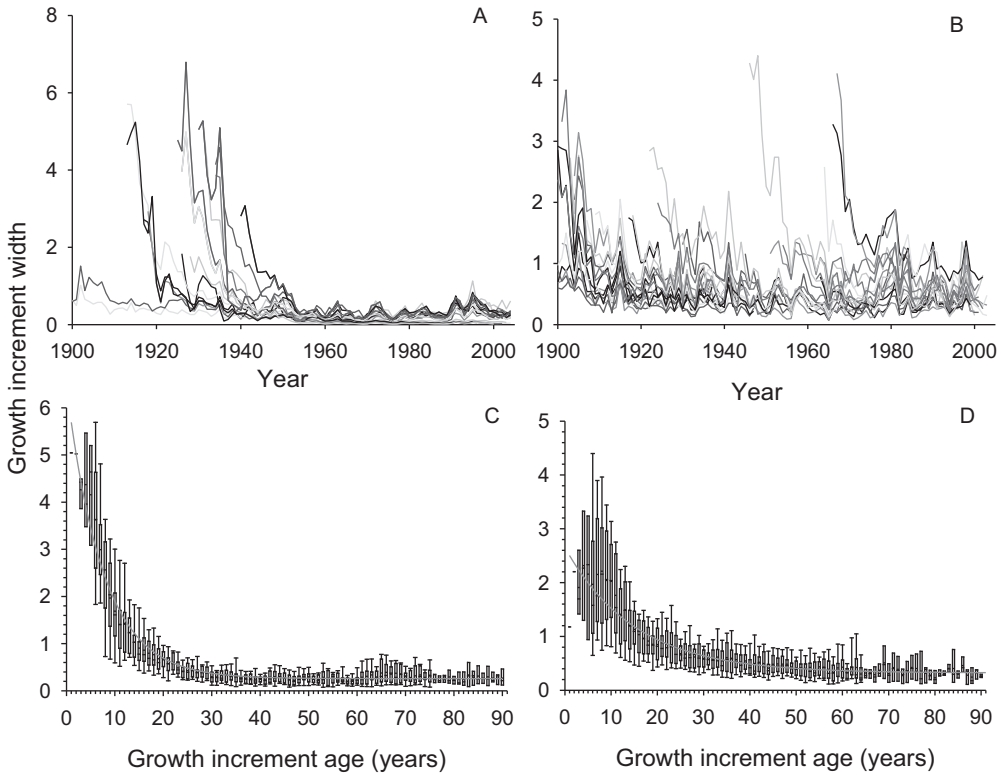

Fig. 2. Pacific geoduck shell growth increment measurements plotted by associated year of growth from specimens taken from the Barkley Sound (A) and Tree Nob (B) sites. Box–Whisker plots of Pacific geoduck growth increment measurements plotted by age of increment formation from the Barkley Sound (C) and Tree Nob (D) sites. Sold line is predicted value from a three parameter negative exponential decay function (Models were fitted by logarithmic transformation of growth increments).

"whitened" measurement time series is then correlated with the average of all others. Any individual with a low correlation ($p < 0.01$) is visually inspected for possible errors and re-measured if any are found. Detailed procedures for COFECHA as well as results of crossdating for Tree Nob were reported in Black et al. (2009). The crossdated Pacific geoduck ages for Tree Nob were recently validated using bomb-radiocarbon ^{14}C methods (Kastelle et al., 2011) for further evidence that all geoduck growth increments were annual and had been exactly dated.

Sea surface temperatures (1942–2003) were obtained from eight lighthouse stations along the British Columbia coast [http://www.pac.dfo-mpo.gc.ca/sci/osap/data/searchtools/Searchlighthouse_e.htm] as well as $2^\circ \times 2^\circ$ gridded SST data available through the International Comprehensive Ocean-Atmosphere Data Set (ICOADS) (http://icoads.noaa.gov/index.shtml). The Pacific Decadal Oscillation (PDO) is defined as the leading principal component of North Pacific monthly SST variability (poleward of 20°N latitude). The PDO is a long-lived El Nino-like pattern of Pacific climate variability with decadal-scale oscillatory warm and cold temperature patterns (Mantua and Hare, 2002) (http://jisao.washington.edu/pdo/PDO.latest). To be consistent with the temporal duration associated with geoduck growth increment data the PDO index for 1900–2003 was used.

2.2. Statistical models

The growth increments at age and at the corresponding year for geoducks sampled from Barkley Sound and Tree Nob showed growth variability between individuals and across the two sites (Fig. 2). An exploratory analysis showed that growth increments (L_{ijk}) of each geoduck can be described by an allometric growth function of age (T_{ijk}); that is, L_{ijk}, where $i = 1, 2, \ldots, n_j$ growth increments at age for individual specimen $j = 1, 2, \ldots, M_k$, and at site $k = 1, 2$ sites for Tree Nob and Barkley sites respectively. This function was linearized by log-transformation of growth increment and age: $y_{ijk} = \alpha_{jk} + \beta_{jk}x_{ijk}$, where $y_{ijk} = \ln(L_{ijk})$, $x_{ijk} = \ln(T_{ijk})$, $\alpha_{jk} = \ln(\alpha_{jk})$, and $\beta_{jk} = b_{jk}$. The estimated α_{jk} and β_{jk} (Fig. 3) showed that age related growth was different among individuals from the two sites. Therefore the baseline hierarchical model (Model 1) was expressed by:

$$y_{ijk} = \alpha_{jk} + \beta_{jk}x_{ijk} + e_{ijk}, \quad (1)$$

where the random errors (e_{ijk}) were assumed to be normally distributed with mean zero and site-specific variance; that is, $e_{ijk} \sim N(0, \sigma^2_{e,k})$. The variation of growth across individuals was modeled by assuming that $\boldsymbol{\theta}_1 = (\alpha_{j1}, \beta_{j1}, \alpha_{j2}, \beta_{j2})$ is a random draw from a multivariate normal distribution (*MVN*) with mean vector $\boldsymbol{\mu} = (\mu_{\alpha 1}, \mu_{\beta 1}, \mu_{\alpha 2}, \mu_{\beta 2})$ and variance–covariance matrix $\mathbf{G} = diag(\mathbf{G}_1, \mathbf{G}_2)$, where $\mathbf{G}_k = \begin{bmatrix} \sigma^2_{\alpha,k} & \sigma_{\alpha\beta,k} \\ \sigma_{\beta\alpha,k} & \sigma^2_{\beta,k} \end{bmatrix}$ for $k = 1, 2$ sites; symbolically, it is $\boldsymbol{\theta}_1 \sim MVN(\boldsymbol{\mu}, \mathbf{G})$. This model accounted for strictly intrinsic age-related growth processes. Thereafter, our modeling strategy was to explore other possible effects from our baseline model on the growth increment data: first by incorporating year-to-year random effects (Model 2); then by incorporating other low-frequency effects such as annual PDO (Model 3); and lastly by a combination of these two effects (Model 4). The order of modeling was unimportant except in the case where all possible effects were combined.

Model (2) added random year-to-year effects into Model (1) to capture all of the unspecified potential environmental factors (e.g., food availability, temperature, water circulations, calcium concentration, etc.) that affect geoduck growth:

$$y_{ijk} = \alpha_{jk} + \beta_{jk}x_{ijk} + \tau_{t,k} + e_{ijk}, \quad (2)$$

where $\tau_{t,k}$ denotes year-to-year environmental effects for $t = 1, \ldots, T$ years in $k = 1, 2$ sites. Year-to-year environmental effects are modeled as random draws from a normal distribution with mean zero and variance $\sigma^2_{h,k}$ across T years in two sites (Weisberg et al., 2010). That is, $\tau_{t,k} \sim N(0, \sigma^2_{h,k})$ for $t = 1, \ldots, T$ years and $k = 1, 2$ sites. This model can be equivalently described by $\tau_{t,k} = 0 + \varepsilon_2$ and $\varepsilon \sim N(0, \sigma^2_{h,k})$ for all years and sites. The predicted random year effect coefficients $\tau_{t,k}$ provided an integrative measure of annual growth variability and were compared to environmental indices to explore climate–growth relationships. The model for year-to-year environmental effects described above can be alternatively expressed by $\boldsymbol{\theta}_2 = (\tau_{t,k}) \sim MVN(\mathbf{0}, \mathbf{H})$ for all T years and two sites, where $\mathbf{H}$ is a $2T \times 2T$ diagonal variance–covariance matrix whose diagonal elements are $\sigma^2_{h,k}$ and off-diagonal are zero. Identical to the Model (1), assume that $\boldsymbol{\theta}_1 \sim MVN(\boldsymbol{\mu}, \mathbf{G})$ and $e_{ijk} \sim N(0, \sigma^2_{e,k})$.

As an alternative to Model (2), systematic effects such as annual PDO were explicitly incorporate into Model (1) using the following equation:

$$y_{ijk} = \alpha_{jk} + \beta_{jk}x_{ijk} + \gamma_{jk}Z_{t|ijk} + e_{ijk}, \quad (3)$$

where $Z_{t|ijk}$ was the value of PDO in year t that corresponded to the ith growth increment of the individual j in site k and $e_{ijk} \sim N(0, \sigma^2_{e,k})$. The coefficient ($\gamma_{jk}$) expressed the long term climate effects of the mean growth response (linear) across both individuals and sites. Because PDO and SST are highly correlated, inclusion of both PDO and SST in the same model may lead to computational difficulties due to colinearity. The PDO was chosen because of its long time series to which growth could be modeled. Similar to Model (1)

$$\boldsymbol{\theta}_1 = (\alpha_{j1}, \beta_{j1}, \gamma_{j1}, \alpha_{j2}, \beta_{j2}, \gamma_{j2})' \sim MVN(\boldsymbol{\mu}, \mathbf{G}), \quad \text{where}$$

$$\boldsymbol{\mu} = (\mu_{\alpha 1}, \mu_{\beta 1}, \mu_{\gamma 1}, \mu_{\alpha 2}, \mu_{\beta 2}, \mu_{\gamma 2})' \quad \text{and}$$

$$\mathbf{G}_k = \begin{bmatrix} \sigma^2_{\alpha,k} & \sigma_{\alpha\beta,k} & \sigma_{\alpha\gamma,k} \\ \sigma_{\beta\alpha,k} & \sigma^2_{\beta,k} & \sigma_{\beta\gamma,k} \\ \sigma_{\gamma\alpha,k} & \sigma_{\gamma\beta,k} & \sigma^2_{\gamma,k} \end{bmatrix}.$$

To evaluate both PDO and random year-to-year effects on growth, Model (1) was expanded to include both factors:

$$y_{ijk} = \alpha_{jk} + \beta_{jk}x_{ijk} + \gamma_{jk}z_{t|ijk} + \tau_{t,k} + e_{ijk} \quad (4)$$

where $\tau_{t,k}$ as that of Model (2), α_{jk}, β_{jk} and γ_{jk} were that of Model (3), and $e_{ijk} \sim N(0, \sigma^2_{e,k})$. We assumed the random errors e_{ijk} of each individual in Models (1)–(4) were uncorrelated. However, additional covariance structure addressing within animal correlation may be specified, and may be particularly useful for growth increment data which represents a time series. For simplicity, the first-order autocorrelation, or AR1 dependence, in the error e_{ijk} was assumed:

$$e_{ijk} = \rho_{jk}e_{i-1,jk} + u_{ijk}$$

where $u_{ijk} \sim N(0, \sigma^2_{u,k})$ was the normally distributed independent random errors, ρ_{jk} was correlation coefficient for the growth increment series of geoduck j in site k, and subscript $i-1$ indicates the age prior to age i. We used the Cochrane–Orcutt transformation (Cochrane and Orcutt, 1949), and applied a stationary AR1 error model (Congdon, 2006; Section 8.5) to Model (4):

$$y_{ijk} = \alpha_{jk} + \beta_{jk}x_{ijk} + \gamma_{jk}z_{t|ijk} + \tau_{t,k} + \rho_{jk}(y_{i-1,jk} - \alpha_{jk} - \beta_{jk}x_{i-1,jk} - \gamma_{jk}z_{t|i-1,jk} - \tau_{t,k}) + u_{ijk} \quad (5)$$

It was assumed that $\rho_{jk} \sim N(\mu_{\rho,k}\sigma^2_{\rho,k})$ and $\mu_{\rho,k} \sim U(-1, 1)$ for $k = 1, 2$ site, where $U(-1, 1)$ is a uniform distribution in $[-1, 1]$.

2.3. Computational aspects using Bayesian inference

In Bayesian statistics, the parameters of hierarchical models can be categorized into model parameters ($\boldsymbol{\theta}$) which include $\boldsymbol{\theta}_1$ and/or $\boldsymbol{\theta}_2$ depending on the model of interest and hyperparameters ($\boldsymbol{\Phi}$) which are the parameters of prior distributions for $\boldsymbol{\theta}$. The joint posterior distribution for ($\boldsymbol{\theta}$, $\boldsymbol{\Phi}$) given a set of data $\mathbf{y}$ is defined as:

$$p(\boldsymbol{\theta}, \boldsymbol{\Phi}|\mathbf{y}) \propto p(\boldsymbol{\theta}, \boldsymbol{\Phi})p(\mathbf{y}|\boldsymbol{\theta}, \boldsymbol{\Phi}) = p(\boldsymbol{\Phi})p(\boldsymbol{\theta}|\boldsymbol{\Phi})p(\mathbf{y}|\boldsymbol{\theta}, \boldsymbol{\Phi})$$

where $(\boldsymbol{\theta}, \boldsymbol{\Phi}) = p(\boldsymbol{\Phi})p(\boldsymbol{\theta}|\boldsymbol{\Phi})$ is the joint prior distribution of vector ($\boldsymbol{\theta}$, $\boldsymbol{\Phi}$) and $p(\mathbf{y}|\boldsymbol{\theta}, \boldsymbol{\Phi})$ is known as likelihood (Gelman et al., 2004).

We were interested in two types of inference: (i) the posterior distribution of the parameters describing the growth curve for each individual with data in the analysis and (ii) inferences for individuals or segments of growth increment data not included in the current analysis (Minte-Vera et al., 2005). For the first inference:

$$p(\boldsymbol{\theta}_i|\mathbf{y}) \propto \int_{\phi} p(\boldsymbol{\theta}_i, \phi|\mathbf{y})d\phi. \quad (6)$$

By integrating out the hyperparameters, which depend on the data for all of the individuals within a site, this model framework lends strength of inference across individuals or individuals within groups. The predictive posterior distribution specified above is conditional on the observed data or probability of the likelihood, and can be used to check whether the model is consistent with the observed data (Gelman et al., 2004). Here, we computed the posterior p-value given as $P(D(y^{\text{rep}},\boldsymbol{\theta}) > D(\mathbf{y},\boldsymbol{\theta})|\mathbf{y})$ as a goodness-of-fit measure (Meng, 1994), where $D(y^{\text{rep}},\boldsymbol{\theta})$ and $D(\mathbf{y},\boldsymbol{\theta})|\mathbf{y}$ are the distributions of the replicated and observed data, respectively. Posterior p-values around 0.5 indicate that the distributions of replicated and actual data are close, while values near zero or one indicate discrepancy between them. The posterior distribution of the parameters for a new set of growth increment measurements not used in the model θ was:

$$p(\tilde{\boldsymbol{\theta}}|\mathbf{y}) \propto \int_{\phi}\int_{\theta} p(\tilde{\boldsymbol{\theta}}|\phi)p(\boldsymbol{\theta}, \phi|\mathbf{y})d\boldsymbol{\theta}\, d\phi. \quad (7)$$

The formulation of the posterior prediction accounts for all uncertainty associated with hyperparameters, parameters and likelihood. Specifically this formulation of the posterior predictive distribution can be used to cross-validate the model when a subset of the data are withheld and the model prediction is generated and compared to observations of growth increment data and environmental indices.

To fit the model to the data using a Bayesian approach, prior probability distributions for the hyperparameters need to be specified. Smith and Wakefield (1994) suggest priors should be noninformative to ensure that the likelihood dominates the prior. We endorsed this approach since no study to date had elicited prior information on the growth increment hyperparameters. As such, the priors for $\boldsymbol{\mu}$ were diffuse multivariate normal distributions, with zero mean and covariance matrix with diagonal elements equal to 1000, and off-diagonal elements equal to zero. The prior for $\mathbf{G}$ was specified by an inverted Wishart distribution (Von Rosen, 1997), with mean matrix of $0.1\mathbf{I}$ and precision matrix of $10^{-6}\mathbf{I}$, where $\mathbf{I}$ was the identity matrix. Instead of using flat Gamma priors for $\sigma_{e,k}^{-2}$ and $\sigma_{e,k}^{-2}$ as recommended by Spiegelhalter et al. (2003), uniform priors with lower and upper boundaries of 0 and 100 respectively are specified to $\sigma_{h,k}$ and $\sigma_{e,k}$ (Kery, 2010). The uniform distribution as been recommended as an alternative prior since the inverse gamma distribution has a spike near zero and can create problems for low values of $\sigma_{e,k}^2$ or $\sigma_{h,k}^2$ (Browne and Draper, 2006). We found that the Markov Chain Monte Carlo (MCMC) simulation traversed the sample space more efficiently with the uniform prior.

WinBUGS (Lunn et al., 2000) was used to fit the model to the data. The estimates of parameters were evaluated based on 500,000 samples after 5000 burn-in samples, thinning to one draw every 20th sample, from MCMC simulation of the joint posterior distribution. Multiple Bayesian diagnostic procedures were performed to evaluate convergence of the MCMC simulation to a stationary posterior distribution for all estimated quantities in the model (Cowles and Carlin, 1996; Brooks and Gelman, 1997). We monitored autocorrelation at various lags to assess whether adequate burn-in and stationarity of the mean had been achieved (Geweke, 1992; Gelman et al., 2004).

The deviance information criterion (DIC), which is conceptually described as goodness of model fit plus model complexity (Spiegelhalter et al., 2002) was used for comparing the competing models. WinBUGS provides DIC with its three computational components, Dbar, pD and Dhat. The deviance, $\boldsymbol{D}(\boldsymbol{\theta}) = -2\,\mathbf{log}(\boldsymbol{p}(\mathbf{y}|\boldsymbol{\theta}))$, is commonly used to measure the goodness of fit (Dempster, 1974), where $\mathbf{y}$ are the data, $\boldsymbol{\theta}$ are the parameters of model, and $\boldsymbol{p}(\mathbf{y}|\boldsymbol{\theta})$ is the likelihood function. Dbar is the posterior mean deviance denoted by $\bar{\boldsymbol{D}} = \boldsymbol{E}[\boldsymbol{D}(\boldsymbol{\theta})]$, which is a measure of how well the model fits the data in Bayesian analysis; the larger this is, the worse the fit. Model complexity (pD) is measured by effective number of parameters, i.e., $\text{pD} = \bar{\boldsymbol{D}} - \boldsymbol{D}(\bar{\boldsymbol{\theta}})$, where $\boldsymbol{D}(\bar{\boldsymbol{\theta}})$ is the deviance evaluated at the posterior mean of the parameters. Dhat ($\tilde{\boldsymbol{D}}(\bar{\boldsymbol{\theta}})$) is a point estimate of $\boldsymbol{D}(\boldsymbol{\theta})$ obtained by substituting $\boldsymbol{\theta}$ with the posterior mean $\bar{\boldsymbol{\theta}}$, that is, $\tilde{\boldsymbol{D}}(\bar{\boldsymbol{\theta}}) = -2\,\log(p(\mathbf{y}|\bar{\boldsymbol{\theta}}))$. In summary, $\text{DIC} = \tilde{\boldsymbol{D}}(\bar{\boldsymbol{\theta}}) + 2\text{pD} = \bar{\boldsymbol{D}} + \text{pD}$. Models with smaller DIC are better supported by the data. Spiegelhalter et al. (2002) suggest that an absolute difference of DIC (ΔDIC), greater than 5 would constitute a substantive difference between two competing models. Spiegelhalter (2006) states that negative DIC is allowed and only ΔDIC is important in model comparison.

3. Results

Growth patterns were strongly synchronous within each of the two sites, facilitating the crossdating process. A statistical check using the program COFECHA verified that dating was accurate and that each increment had been assigned the correct calendar years of formation. After low-frequency processes had been removed, the mean correlation between each individual measurement time series and the average of all others was 0.65 for Barkley and 0.74 for Tree Nob, underscoring the high level of growth synchrony at each site.

The parameters describing the change in growth increment width as a function of age were notably different between the Barkley Sound and Tree Nob (Fig. 3 and Tables 1 and 2). Also, between-individual growth variability within a site and within-site variances was notably greater at Barkley Sound in comparison to Tree Nob (Table 1). For example, once age-related growth was accounted for in the model, remaining variability in growth increment data was twice as large at Barkley Sound ($\sigma_{e,1}^2 = 0.256$) than at Tree Nob ($\sigma_{e,2}^2 = 0.122$) (Table 2). These results suggested that the initial hierarchical model structure (i.e., Model (1)) of treating site-specific mean growth parameters α_k and β_k, variance–covariance matrix ($\sigma_\alpha^2, \sigma_\beta^2$), and within-error variance ($\sigma_{e,k}^2$) was a good starting point for more complex model development. Although not shown in Table 1, this model had a ΔDIC of 2300 when compared to a reduced grand mean model that treated all geoduck from the same site.

Addition of unspecified year-to-year variability, $\sigma_{h,k}^2$, as a random effect resulted in the greatest change in ΔDIC; compared to the Model (1), ΔDIC was 2501 and 482 for Models (2) and (3), respectively (Table 1). Expressed as the proportion of variance explained by additional covariates, $1 - (\sigma_{e,F}^2/\sigma_{e,R}^2)$ where F and R refer to full

Table 1
Bayesian estimates of mean and standard deviation (SD) for the coefficients in Models (1)–(5). $\sigma^2_{e,k}$ is the variance of residual errors e_{ijk} for Models (1)–(4) and $\sigma^2_{u,k}$ is the variance of u_{ijk} for Model (5), where $k = 1$ (Barkley Sound), 2 (Tree Nob) sites.

Coefficient	Model (1)		Model (2)		Model (3)		Model (4)		Model (5)	
	Mean	SD	Mean	SD	Mean	SD	Mean	SD	Mean	SD
Barkley sound										
α_1	2.032	0.294	2.478	0.335	2.007	0.295	2.452	0.329	2.344	0.309
β_1	−0.858	0.081	−0.972	0.090	−0.851	0.081	−0.964	0.089	−0.932	0.084
γ_1	–	–	–	–	0.118	0.040	0.140	0.064	0.105	0.056
ρ_1	–	–	–	–	–	–	–	–	0.666	0.053
$\sigma^2_{\alpha,1}$	1.166	0.505	1.415	0.594	1.172	0.485	1.435	0.577	1.155	0.491
$\sigma^2_{\beta,1}$	0.088	0.038	0.101	0.043	0.088	0.037	0.102	0.041	0.082	0.035
$\sigma^2_{\gamma,1}$	–	–	–	–	0.018	0.008	0.016	0.007	0.010	0.004
$\sigma^2_{\rho,1}$	–	–	–	–	–	–	–	–	0.015	0.016
$\sigma^2_{h,1}$	–	–	0.186	0.028	–	–	0.175	0.027	0.123	0.025
$\sigma^2_{e,1}$ or $\sigma^2_{u,1}$	0.256	0.011	0.077	0.004	0.240	0.010	0.071	0.003	0.051	0.002
Tree Nob										
α_2	2.182	0.173	2.808	0.209	2.319	0.170	2.662	0.200	2.597	0.189
β_2	−0.794	0.048	−0.979	0.056	−0.837	0.047	−0.937	0.054	−0.917	0.051
γ_2	–	–	–	–	0.176	0.023	0.196	0.036	0.185	0.036
ρ_2	–	–	–	–	–	–	–	–	0.356	0.039
$\sigma^2_{\alpha,2}$	0.804	0.264	0.991	0.288	0.782	0.249	0.949	0.280	0.785	0.246
$\sigma^2_{\beta,2}$	0.059	0.020	0.068	0.020	0.057	0.019	0.065	0.020	0.054	0.017
$\sigma^2_{\gamma,2}$	–	–	–	–	0.012	0.004	0.010	0.003	0.010	0.003
$\sigma^2_{\rho,2}$	–	–	–	–	–	–	–	–	0.017	0.014
$\sigma^2_{h,2}$	–	–	0.083	0.013	–	–	0.056	0.009	0.052	0.008
$\sigma^2_{e,2}$ or $\sigma^2_{u,2}$	0.122	0.004	0.051	0.002	0.100	0.004	0.048	0.002	0.044	0.002
DIC	2861.9		360.7		2380.4		212.4		−276.7	

and reduced models, Model (2) accounted for 70% and 58% of the total variability in growth increment data from the base model at Barkley Sound and Tree Nob, respectively. Variances associated with random year effects ($\sigma^2_{h,k}$), which some authors have referred to as an environmental variance term, at both sites were substantially greater than residual within-error variances ($\sigma^2_{e,k}$); Barkley Sound ($\sigma^2_{h,1} = 0.185$; $\sigma^2_{e,1} = 0.077$) being more than twice that of Tree Nob ($\sigma^2_{h,2} = 0.082$; $\sigma^2_{e,2} = 0.051$) (Table 1). Intraclass correlation, $\sigma^2_{h,k}/[\sigma^2_{h,k} + \sigma^2_{e,k}]$, which represents the correlation between growth increments measured among all individuals in the sample, was 0.72 and 0.62 for Tree Nob and Barkley Sound, respectively.

Annual growth increment variability is illustrated in Figs. 4 and 5 by plotting the credible interval of the random year effect coefficients from the Bayesian hierarchical Model (2). Geoduck growth at both Barkley Sound and Tree Nob showed reasonably strong coherence with climate variables, SST and PDO anomaly (Figs. 4 and 5). In general, geoduck growth was below average during periods of low PDO and SST, while growth was greater than average during high PDO and SST. This coherence was particularly evident during the sustained cool regime in the North Pacific starting at about 1945, followed by a shift to a warm regime during the late 1970s (Figs. 4 and 5). While geoduck growth from the two sites seemed to track each other fairly well, there were notable exceptions such as a period of below average growth at Tree Nob between 1908 and 1920, corresponded to a brief period of low PDO. The Tree Nob growth increment index also seemed to capture the rapid high-low and low-high transitions in PDO regimes over the last half century better than geoduck at Barkely Sound.

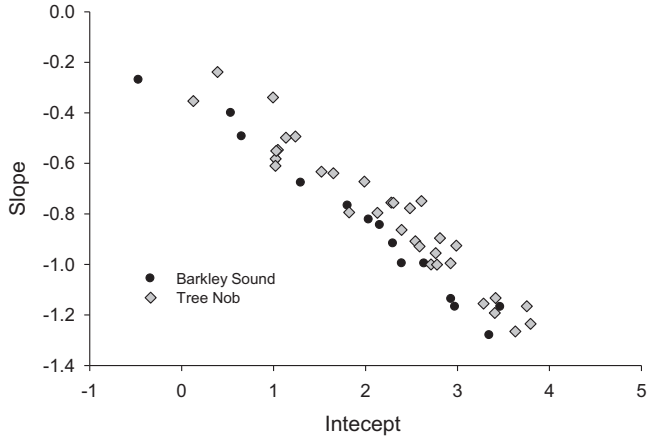

Fig. 3. Bayesian hierarchical geoduck growth increment model parameter coefficients (α_k,β_k) by site of collection illustrates a better fit to the data is achieved when the model explicitly accounts for site differences.

Explicitly accounting for climate variability in growth showed that PDO was a good predictor of the geoduck growth increment data. We focused on PDO, rather than SST, because PDO had a much longer historical record consistent with the geoduck time series, and both environmental indices were highly correlated. As a relative change from Model (1), the ΔDIC was 481.5 suggesting that PDO explained significantly more growth variability than intrinsic age-related effects alone (Table 1). Correlations between PDO index and predicted growth increments (Figs. 4 and 5) from Model (2) illustrate this relationship. Model (3) includes PDO as a predictor with the expected linear mean response positively related to the PDO anomaly at both Barkley Sound and Tree Nob ($\gamma_1 = 0.118$, $\gamma_2 = 0.176$, respectively) (Table 1). With no posterior density on zero, as indicated by Bayesian credibility intervals, these results indicate these relationships (slopes) are significantly different from zero (Table 2). The PDO series was a better predictor of geoduck growth at Tree Nob than Barkley Sound; total variability in the growth increment was 6% and 19% for Barkley Sound and Tree Nob, respectively. It should be noted, however, that Model (3) explained comparatively less of the total variability in geoduck growth increment data than Model (2).

We further evaluated whether improvements in fit could be obtained by including both the random year effect and long-term climate effects (PDO), once age-related growth was accounted for (i.e., Model (4)). This model showed significant improvement in fit to the data when compared to either Model (2) or Model (3)

Table 2
Bayesian estimates of median and two-tailed 5% credential interval for the coefficients in Models (1)–(5). $\sigma^2_{e,k}$ is the variance of residual errors e_{ijk} for Models (1)–(4) and $\sigma^2_{u,k}$ is the variance of u_{ijk} for Model (5), where k = 1 (Barkley Sound), 2 (Tree Nob) sites.

Coefficient	Model (1)			Model (2)			Model (3)			Model (4)			Model (5)		
	Median	2.5%	97.5%	Median	2.5%	97.5%	Median	2.5%	97.5%	Median	2.5%	97.5%	Median	2.5%	97.5%
Barkley sound															
α_1	2.031	1.456	2.617	2.477	1.821	3.143	2.007	1.424	2.589	2.451	1.793	3.106	2.344	1.737	2.957
β_1	−0.858	−1.019	−0.700	−0.971	−1.152	−0.793	−0.851	−1.009	−0.690	−0.963	−1.141	−0.788	−0.932	−1.099	−0.770
γ_1	–	–	–	–	–	–	0.118	0.039	0.194	0.141	0.017	0.265	0.105	−0.003	0.217
ρ_1	–	–	–	–	–	–	–	–	–	–	–	–	0.667	0.558	0.769
$\sigma^2_{\alpha,1}$	1.062	0.517	2.418	1.292	0.671	2.887	1.074	0.538	2.400	1.316	0.684	2.859	1.053	0.516	2.406
$\sigma^2_{\beta,1}$	0.080	0.039	0.184	0.092	0.047	0.206	0.081	0.040	0.181	0.093	0.048	0.205	0.075	0.036	0.171
$\sigma^2_{\gamma,1}$	–	–	–	–	–	–	0.016	0.008	0.040	0.015	0.007	0.033	0.009	0.005	0.021
$\sigma^2_{\rho,1}$	–	–	–	–	–	–	–	–	–	–	–	–	0.010	0.000	0.058
$\sigma^2_{h,1}$	–	–	–	0.184	0.139	0.248	–	–	–	0.172	0.130	0.235	0.121	0.079	0.176
or $\sigma^2_{u,1}$ $\sigma^2_{e,1}$	0.256	0.236	0.279	0.076	0.070	0.084	0.240	0.220	0.261	0.071	0.065	0.077	0.051	0.046	0.056
Tree Nob															
α_2	2.181	1.842	2.527	2.809	2.396	3.224	2.319	1.985	2.658	2.662	2.272	3.058	2.595	2.227	2.973
β_2	−0.794	−0.889	−0.701	−0.979	−1.090	−0.869	−0.837	−0.931	−0.745	−0.937	−1.043	−0.833	−0.916	−1.019	−0.817
γ_2	–	–	–	–	–	–	0.176	0.131	0.221	0.196	0.124	0.267	0.184	0.115	0.255
ρ_2	–	–	–	–	–	–	–	–	–	–	–	–	0.356	0.276	0.429
$\sigma^2_{\alpha,2}$	0.762	0.413	1.441	0.946	0.561	1.682	0.743	0.414	1.370	0.903	0.536	1.624	0.745	0.423	1.375
$\sigma^2_{\beta,2}$	0.056	0.030	0.108	0.065	0.038	0.117	0.054	0.029	0.103	0.062	0.036	0.113	0.051	0.028	0.096
$\sigma^2_{\gamma,2}$	–	–	–	–	–	–	0.012	0.007	0.021	0.010	0.006	0.018	0.010	0.006	0.017
$\sigma^2_{\rho,2}$	–	–	–	–	–	–	–	–	–	–	–	–	0.013	0.000	0.051
$\sigma^2_{h,2}$	–	–	–	0.082	0.062	0.111	–	–	–	0.055	0.041	0.075	0.051	0.038	0.070
or $\sigma^2_{u,2}$ $\sigma^2_{e,2}$	0.122	0.114	0.132	0.051	0.047	0.055	0.100	0.093	0.107	0.048	0.044	0.052	0.044	0.041	0.047

with ΔDIC = 148.3 and 2168.0, respectively (Table 1). The variance associated with the climate effect, PDO ($\sigma^2_{\gamma,k}$), was estimated to be 0.016 and 0.010 at Barkley sound and Tree Nob sites, respectively (Table 2). Climate induced variability in the growth increment data accounted for approximately 18% of the remaining residual within-error variance $\sigma^2_{\gamma,k}/[\sigma^2_{\gamma,k+\sigma^2_{e,k}}]$ at both Barkley Sound and Tree Nob sites. While random year-to-year variability was the dominant variance component at these sites, comparatively more variability was explained with the addition of the climate term in the model at Tree Nob than compared to Barkley Sound. Again growth increment variation as a function of age was strongly related to the PDO anomaly, with the Tree Nob site showing a comparatively stronger positive response ($\gamma_2 = 0.196$) than Barkley Sound ($\gamma_1 = 0.141$). In other words, the rate of change in shell increment width as a function of age (slope) was less negative during years with greater PDO values. The inclusion of an AR1 error structure to Model (4) (i.e., Model (5)) resulted in a ΔDIC = 489.1. While this change in model's error structure did produce a relatively large reduction in DIC, the differences in model parameter and variance estimates were small (Table 2).

The MCMC simulation using the Gibbs sampler was computationally efficient, yielding approximately 25,000 samples with which to compute summary statistics and develop a framework for model building and hypothesis tests. Initial testing of the MCMC simulation showed burn-in was achieved after only 5000 samples and between-sample autocorrelation of estimated parameters was non-significant after a lag of 20 sample parameter sets. Thus, a sample retention rate of 1 in every 20 MCMC draws was more than adequate to ensure independence. While not shown for all parameters, trace plots for selected variance components (i.e., year-to-year variability, $\sigma^2_{h,k}$) showed good mixing and reasonable evidence that the chain had converged to a stationary distribution (Fig. 6). Kernel densities appeared uni-modal and relatively smooth, suggesting that MCMC sampling traversed the parameter space effectively. Further evidence of convergence was shown by the Geweke (1992) test statistics.

The posterior predictive distribution derived from the MCMC sample showed that the model (i.e., Model (4)) was consistent with the observed growth increment data. Rather than summarizing the posterior to a test quantity and comparing it to the same quantity of the observed data, we simply calculated the distribution of tail probabilities (posterior p-values) corresponding to the integral of the posterior predictive distribution up to the observed value. Unusually large numbers of small or large tail probabilities would suggest model misfit. In this instance, the greatest density of tail probabilities centered on 0.5–0.55 and monotonically declined toward zero and 1.0 (Fig. 7). In fact, the number of tail probabilities less than 0.05 and greater than 0.95 was approximately the number expected to deviate outside of the posterior credible interval by chance alone. Overall, these results suggested that the model fit the data well.

4. Discussion

The modeling approach presented here uses contemporary statistical methods and software to analyze growth increment data in marine organisms. In particular, we advocate the use of Bayesian hierarchical methods to model the intrinsic age-related and extrinsic environmental effects on growth. The number of studies analyzing growth increment data in fish, bivalves and other marine animals and its relationship to environmental variability has increased (Boehlert et al., 1989; Strom et al., 2004; Black et al., 2009) in recent years. Statistically integrated modeling approaches, such as hierarchical Bayesian or mixed-effects models, produce advantages that include hypothesis testing, exploration of age and

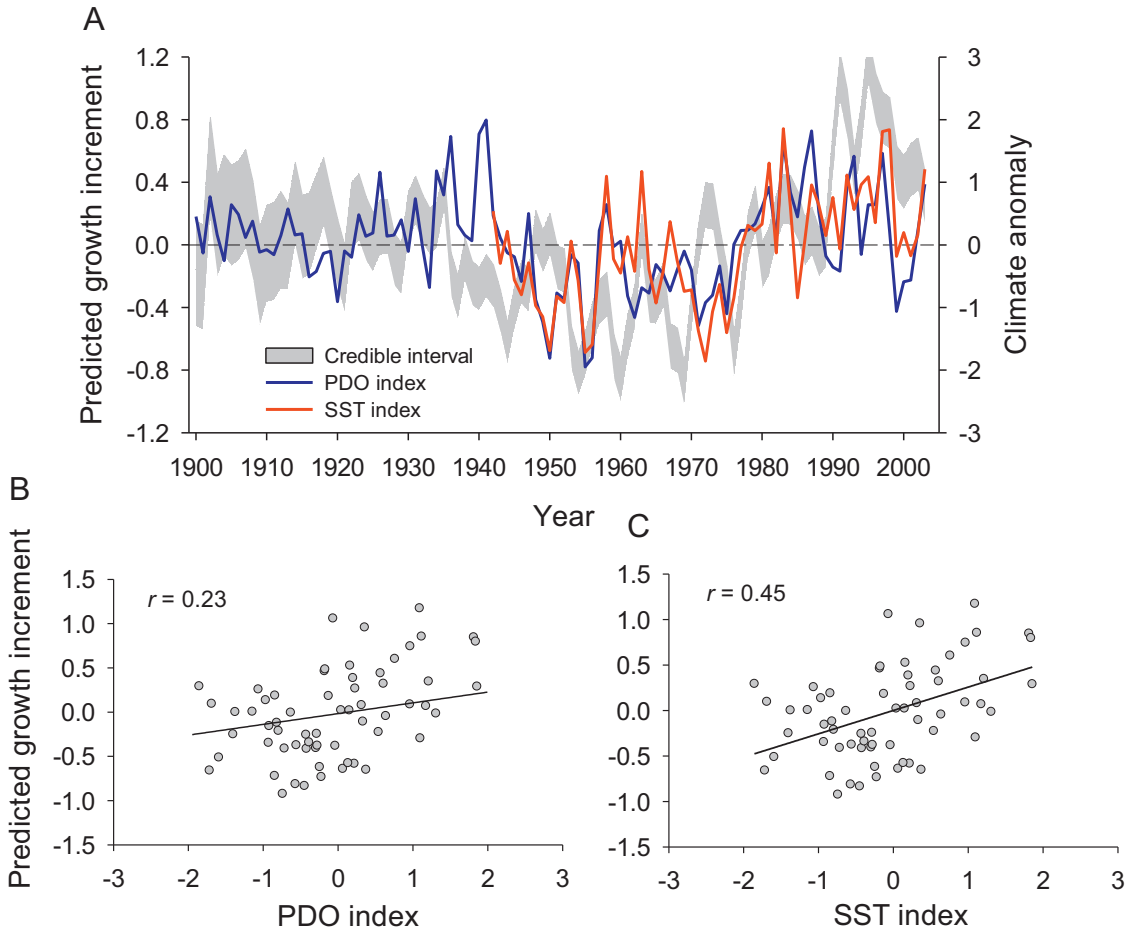

Fig. 4. (A) Predicted annual growth increment for Barkley Sound geoduck. The index is the random year effect estimates, $\tau_{t,k} \sim N(0, \sigma^2_{h,k})$, from the Bayesian hierarchical growth model (model (2)) and is expressed as the credible interval of that effect. Climate indices of annual sea surface temperature (SST) and Pacific Decadal Oscillation (PDO) anomalies are overlaid with the predicted growth increment to show coherence between geoduck growth and climate factors.

climate effects on both short- and long-term growth, and explicit estimation of all relevant variance components. The hierarchical model allows for conditional mean response in age-related growth over all individual times series at different sites (or species), explicitly captures the low-frequency climate forcing on the intrinsic growth rates, and is able to preserve trends in excess of the lengths of any individual time series through the statistical process known as "shrinkage".

There is a straight-forward connection between the "standard" chronology developed in dendrochronology procedures (ARSTAN program) (Cook, 1985) and the random year effect coefficients ($\tau_{t,k} \sim N(0, \sigma^2_{h,k})$) from the Bayesian hierarchical model, which naturally includes posterior prediction intervals that are generated without further calculations. This was confirmed by a high correlation ($r > 0.90$) between our estimate using the Bayesian hierarchical approach and the chronology of Black et al. (2009) using traditional dendrochronology methods. Also, explicitly modeling non-stationary effects on growth (i.e., PDO), while accounting for age-related effects and random year effects, such as Model (4), preserves long-term trends that might otherwise be lost and is essentially the analog to Regional Curve Standardization (RCS) in Tree-ring Science (Esper et al., 2002). Furthermore, the hierarchical Bayesian model also estimates the intraclass correlation (Gelman et al., 2004), $\sigma^2_{h,k}/[\sigma^2_{h,k} + \sigma^2_{h,k}]$, which is equivalent to series intercorrelation generated from ARSTAN.

Application of hierarchical methods is very natural since growth increment data are inherently grouped into different levels of organization (repeated growth increment measurements within subject, subject within population or species), and covariates are available at different levels of variation (Gelman et al., 2004). Such types of data sets are ubiquitous in the natural sciences where a record of historical annual growth is contained in discrete and often highly identifiable increments, including tree xylem (Fritz, 1976), coral calcium carbonate (Correge, 2006), fish otoliths (Campana and Thorrold, 2001), and bivalve shells (Noakes and Campbell, 1992). Fisheries science has a long tradition of growth increment analysis that has focused on the back-calculation of growth histories of fishes (Whitney and Carlander, 1956), including a diverse array of statistical procedures to fit the growth data (Francis, 1990). More recently, fisheries scientists have increasingly used more sophisticated hierarchical approaches for estimating growth variability in fish, both at the individual (Pilling et al., 2002) and population levels (Helser and Lai, 2004). Tree-ring scientists have also begun using integrative statistical methods to quantify the contribution of a common high frequency signal hidden among ring-width time series (Boreux et al., 2009; Li et al., 2010). The approach presented in this paper bears some resemblance to Weisberg et al. (2010) who analyzed growth increment data using factorized linear mixed effects models. However, the Bayesian hierarchical methods used in our approach allows for both linear and nonlinear growth related effects, explicitly models changes in growth as influenced by climate processes, fully characterized uncertainty from both intrinsic and extrinsic (environmental effects) through MCMC integration, and has the ability to use latent variables to capture prediction

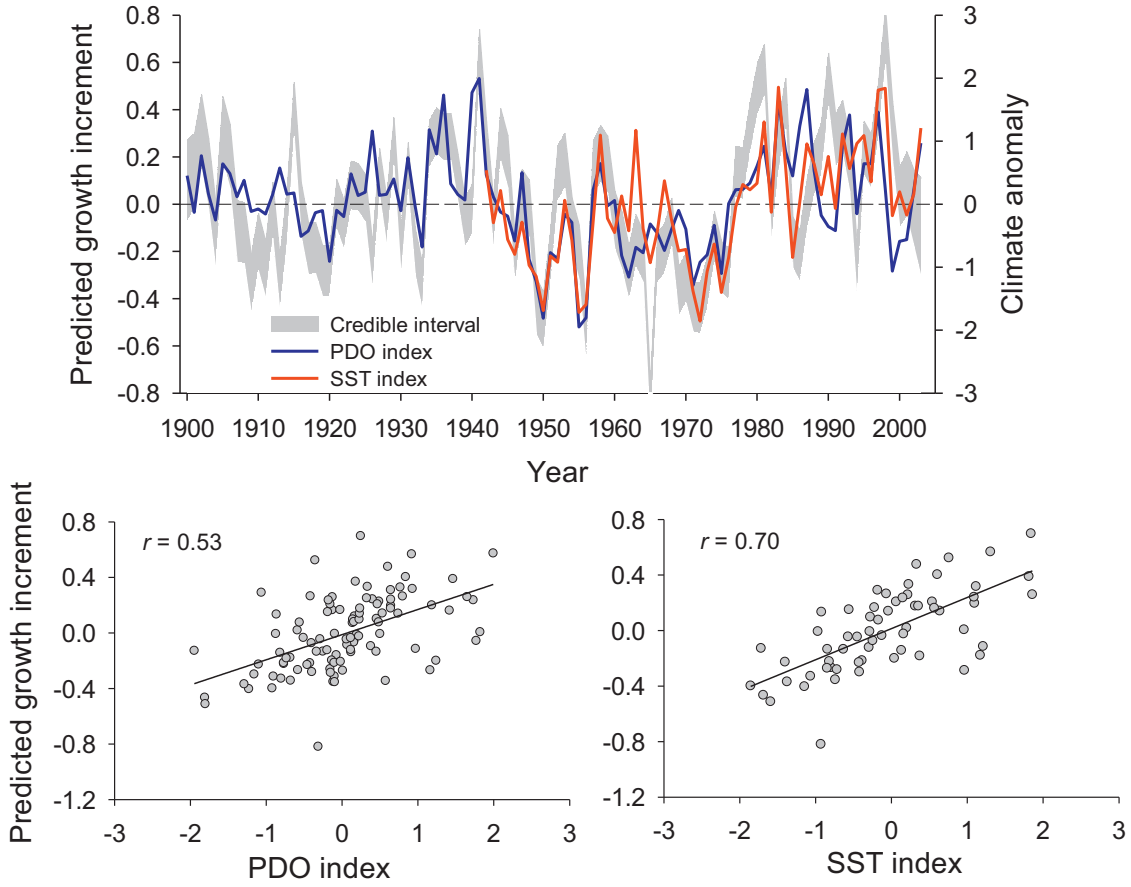

Fig. 5. (A) Predicted annual growth increment for Tree Nob geoduck. The index is the random year effect estimates, $\tau_{t,k} \sim N(0, \sigma^2_{h,k})$, from the Bayesian hierarchical growth model (model (2)) and is expressed as the credible interval of that effect. Climate indices of annual sea surface temperature (SST) and Pacific Decadal Oscillation (PDO) anomalies are overlaid with the predicted growth increment to show coherence between geoduck growth and climate factors.

uncertainty for historical environmental reconstruction. The latter advantage has been demonstrated by Li et al. (2010). Equipped with these statistical tools ecologists have a rigorous framework to study the relationship between environmental and climate variability and their effects on animal growth over diverse taxa in marine systems.

To account for autocorrelation in the error structure of the model, we assumed a first-order autoregressive process (AR1) in the error structure and found little change in parameter and variance estimates even though a much smaller ΔDIC was observed. Little difference between estimates of model effects suggests the model is robust to the covariance structure assumed (Zeger and Liang, 1986). However, this study does not address the question on whether or not to consider a high-order autocorrelation ARp errors, for $p \geq 2$. During the course of analysis, we found the inclusion of AR1 error structure in the models takes substantially more computational time and longer MCMC iterations to reach convergence. Computational resources may need to be weighed against more complicated error structures. Also, models may be over-parameterized if higher-order autocorrelated errors are involved. There are many other ways to formulize AR1 error into models (see Congdon, 2006) that have not been explored in this article. It is of interest in the future to explore the differences caused by various formulizations.

Pacific geoduck growth increment widths, and potentially isotopic properties, represent a valuable climate archive (Strom et al., 2004; Goman et al., 2008; Hallmann et al., 2008). In the analysis presented here we concur with previous studies that climate variability through PDO exerts a significant influence on geoduck growth rates. While not explicitly tested in the hierarchical mixed effects model, SST probably accounts for much of this variability since positive correlations in the growth of other marine bivalves and water temperature have been demonstrated in the laboratory (Cerrato, 2000). Specifically for geoduck, correlations between growth increment width in the shells and water temperature have been found in field studies (Noakes and Campbell, 1992).

Variances associated with PDO were comparatively less than interannual variance components, but nevertheless indicated that PDO had a strong impact on average age-related growth rates of geoduck. These findings indicate that, in addition to high-frequency variation in regional sea surface temperatures, basin-scale processes such as the Pacific Decadal Oscillation are strong controlling factors of geoduck metabolic rates and shell accretion. Geoduck growth rates at Tree Nob, in particular, showed greater teleconnections to regional and basin-scale oceanographic processes than Barkley Sound. Black et al. (2009) found a similar lack of correlation between SST and geoduck at Cape Mark and Brady's Beach sites, which are in close proximity to Barkley Sound. Some sites may be more heavily influenced by local environmental processes, as would be expected in the heterogeneous nearshore environment of the British Columbia coast (Black et al., 2009). Yet, despite decoupling between regional temperature and growth at interannual timescales at Barkley, Pacific geoduck contain residual variance that corresponds with multidecadal "regime shifts" from warm to cool phases of the PDO. This may reflect PDO-related influences over ocean circulation or productivity, which could amplify climate signals in geoduck growth. Regardless of the mechanism, geoduck captures local and broad-scale patterns of climate variability in the

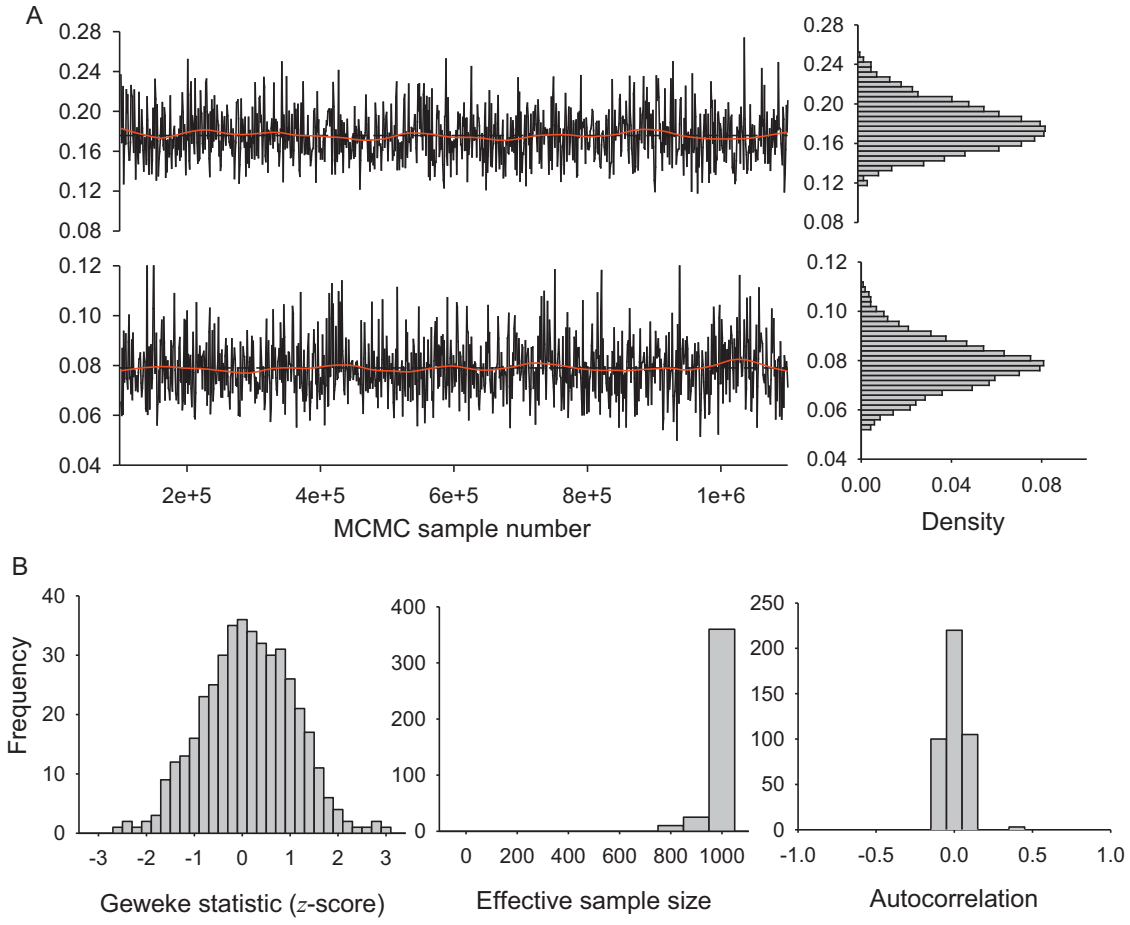

Fig. 6. Markov Chain Monte Carlo (MCMC) convergence diagnostics of Bayesian hierarchical growth model for Barkley Sound and Tree Nob geoduck fit in WinBUGs software. Top panel (A) show trace plots of the year effect variances (σ_h^2) for Tree Nob geoduck. Bottom three panels (B) show Geweke statistics, effective sample sizes and autocorrelation of all model parameters. Results provide strong evidence that model converged to a stationary posterior target distribution.

North Pacific. Also, our results with geoduck add to a growing body of literature documenting PDO-related biophysical coupling over numerous taxa in the North Pacific Ocean (Hollowed et al., 1998; Mantua and Hare, 2002; Martinez et al., 2009).

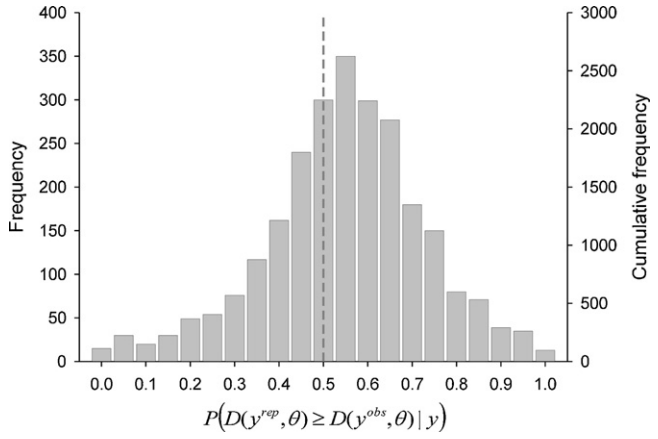

Fig. 7. Posterior *P*-value, calculated as $P(D(y^{rep},\theta) \geq D(y^{obs},\theta)|y)$, compares the distribution of replicated data (posterior distribution) to the observed data as a Bayesian measure of goodness-of-fit. Values close to 0.5 indicate that the distributions of replicated and actual data are close, while values close to zero or one indicate differences between them.

References

Bernard, F.R., 1983. Catalog of the living Bivalvia of the eastern Pacific Ocean: Bering Strait to Cape Horn. Canadian Special Publication of Fisheries and Aquatic Sciences, p. 61.

Black, B.A., Boehlert, G.W., Yoklavich, M.M., 2008a. Establishing climate–growth relationships for yelloweye rockfish (*Sebastes ruberrimus*) in the northeast Pacific using a dendrochronological approach. Fisheries Oceanography 17, 368–379.

Black, B.A., Gillespie, D.C., MacLellan, S.E., Hand, C.M., 2008b. Establishing highly accurate production-age data using the tree-ring technique of crossdating: a case study for Pacific geoduck (*Panopea abrupta*). Canadian Journal of Fisheries and Aquatic Sciences 65, 2572–2578.

Black, B.A., Copenheaver, C.A., Frank, D.C., Stuckey, M.J., Kormanyos, R.E., 2009. Multi-proxy reconstructions of northeastern Pacific sea surface temperature data from trees and Pacific geoduck. Palaeogeography, Palaeoclimatology and Palaeoecology 278, 40–47.

Boehlert, G.W., Yoklavich, M.M., Chelton, D.B., 1989. Time-series of growth in the genus *Sebastes* from the northeast Pacific-Ocean. Fishery Bulletin 87, 791–806.

Boreux, J.-J., Naveau, P., Guin, O., Perreault, L., Bernier, J., 2009. Extracting a common high frequency signal from Northern Quebec black spruce tree-rings with a Bayesian hierarchical model. Climate of the Past 5, 607–613.

Brooks, S., Gelman, A., 1997. General methods for monitoring convergence of iterative simulations. Journal of Computational and Graphical Statistics 7, 434–455.

Browne, W.J., Draper, D., 2006. A comparison of Bayesian and likelihood-based methods for fitting multilevel models. Bayesian Analysis 1, 473–550.

Bunn, A.G., Sharac, T.J., Graumlich, L.J., 2004. Using a simulation model to compare methods of tree-ring detrending and to investigate the detectability of low-frequency signals. Tree-Ring Research 60 (2), 77–90.

Butler, P.G., Richardson, C.A., Scourse, J.A., Wanamaker Jr., A.D., Shammon, T.M., Bennell, J.D., 2009. Marine climate in the Irish Sea: analysis of a 489-year marine master chronology derived from growth increments in the shell of the clam *Arctica islandica*. Quaternary Science Reviews 29, 1614–1632.

Campana, S.E., Thorrold, S.R., 2001. Otoliths, increments, and elements: keys to a comprehensive understanding of fish populations? Canadian Journal of Fisheries and Aquatic Sciences 58, 30–38.

Cerrato, R.M., 2000. What fish biologists should know about bivalve shells. Fisheries Research 46, 39–49.
Coan, E.V., Scott, P.V., Bernard, F.R., 2000. Bivalve Shells of the Western North America. Santa Barbara Museum of Natrual History, Santa Barbara.
Cochrane, D., Orcutt, G.H., 1949. Application of least squares regression to relationship containing autocorrelated error terms. Journal of the American Statistical Association 44, 32–61.
Congdon, P., 2006. Bayesian Statistical Modelling, 2nd ed. John Wieley & Sons, West Sussex, England.
Cook, E.R., 1985. A time-series analysis approach to tree-ring standardization. Ph.D. Thesis. University of Arizona.
Cook, E.R., Briffa, K.R., Meko, D.M., Graybill, D.A., Funkhouser, G., 1995. The 'segment length curse' in long tree-ring chronology development for paleoclimatic studies. The Holocene 5, 229–237.
Cook, E.R., Kairiukstis, L.A., 1990. Methods of Dendrochronology: Applications in the Environmental Sciences. Springer-Verlag, NY.
Correge, T., 2006. Sea surface temperature and salinity reconstruction from coral geochemical tracers. Palaeogeography, Palaeoclimatology and Palaeoecology 232, 408–428.
Cowles, M.K., Carlin, B.P., 1996. Markov Chain Monte Carlo convergence diagnostics: a comparative review. Journal of the American Statistical Association 91, 883–904.
Dempster, A.P., 1974. The direct use of likelihood for significance testing. In: Barnforff-Nielsen, O., Blaesild, P., Schou, G. (Eds.), Proc. Foundational Questions in Statistical Inference. University of Aarhus, pp. 335–352.
Eronen, M., Zetterberg, P., Briffa, K., Lindholm, M., Meriläinen, J., Timonen, M., 2002. Part 1: the supra-long Scots pine tree-ring record for northern Finnish Lapland; Chronology construction and initial inferences. The Holocene 12, 673–680.
Esper, J., Cook, E.R., Schweingruber, F.H., 2002. Low-frequency signals in long tree-ring chronologies for reconstructing past temperature variability. Science 295, 2250–2253.
Ferguson, C.W., 1968. Bristlecone pine: science and esthetics. Science 159, 839–846.
Francis, R.C., Hare, S.R., 1994. Decadal-scale regime shifts in the large marine ecosystems of the North-east Pacific: a case for historical science. Fisheries Oceanography 3, 279–291.
Francis, R.I.C.C., 1990. Back-calculation of fish length: a critical review. Journal of Fish Biology 36 (6), 883–902.
Fritz, H.C., 1976. Tree Rings and Climate. Academic Press, New York.
Gelman, A., Carlin, J.B., Stern, H.S., Rubin, D.B., 2004. Bayesian Data Analysis, 2nd ed. Chapman and Hall, New York, NY.
Geweke, J., 1992. Evaluating the accuracy of sampling-based approaches to the calculation of posterior moments. In: Bernardo, J.M., Berger, J., Dawid, A.P., Smith, A.F.M. (Eds.), Bayesian Statistics 4. Oxford University Press, Oxford.
Goman, M., Ingram, B.L., Strom, A., 2008. Composition of stable isotopes in geoduck (*Panopea abrupta*) shells: a preliminary assessment of annual and seasonal paleoceanographic changes in the northeast Pacific. Quaternary International 188, 117–125.
Hagen, P.T., Quinn, T.J., 1991. Long-term growth dynamics of young Pacific halibut: evidence of temperature-induced variation. Fisheries Research 11, 283–306.
Hallmann, N., Schone, B.R., Strom, A., Fiebig, J., 2008. An intractable climate archive – Sclerochronological and shell oxygen isotope analyses of the Pacific geoduck from Protection Island (Washington State, USA). Palaeogeography, Palaeoclimatology and Palaeoecology 269, 115–126.
Helser, T.E., Lai, H-L., 2004. A Bayesian hierarchical meta-analysis of fish growth: with an example for North American largemouth bass, *Micropterus salmoides*. Ecological Modelling 178, 399–416.
Helser, T.E., Stewart, I.J., Lai, H-L., 2007. A Bayesian hierarchical meta-analysis of growth for the genus *Sebastes* in the eastern Pacific Ocean. Canadian Journal of Fisheries and Aquatic Sciences 64, 470–485.
Hollowed, A.B., Hare, S.R., Wooster, W.S., 1998. Pacific-basin climate variability and patterns in the Northeast Pacific marine fish production. In: Wolloway, G., Muller, P., Henderson, D. (Eds.), Proceedings of the 10th 'Aha Huliko' a Hawaiian Winter Workshop on Biotic Impacts of Extratropical Climate Variability in the Pacific. NOAA, SOEST Special Publication, pp. 89–104.
Kastelle, C.R., Helser, T.E., Black, B.A., Stuckey, M.J., Gillespie, D.C., McArthur, J., Little, D., Charles, K.D., Khan, R.S., 2011. Bomb-produced radiocarbon validation of growth-increment crossdating allows marine paleoclimate reconstruction. Palaeogeography, Palaeoclimatology and Palaeoecology 311, 126–135.
Kery, M., 2010. Introduction to WinBUGS for Ecologists: Bayesian Approach to Regression, ANOVA, Mixed Models and Relative Analyses. Academic Press, NY.
Killingley, J.S., Berger, W.H., 1979. Stable isotopes in a mollusk shell – detection of upwelling events. Science 205, 186–188.
Krantz, D.E., Williams, D.F., Jones, D.S., 1987. Ecological and paleoenvironmental information using table isotope profiles from living and fossil mollusks. Palaeogeography, Palaeoclimatology and Palaeoecology 58, 249–266.
Li, B., Nychka, D.W., Ammann, C.M., 2010. The value of multiproxy reconstruction of past climate. Journal of the American Statistical Association 105 (491), 883–895.
Lunn, D.J., Thomas, A., Best, N., Spiegelhalter, D., 2000. WinBUGS – a Bayesian modelling framework: concepts, structure, and extensibility. Statistics and Computing 10, 325–337.
Mantua, H.J., Hare, S.R., 2002. The Pacific decadal oscillation. Journal of Oceanography 58, 35–44.
Marchitto, T.M., Jones, G.A., Goodfriend, G.A., Weidman, C.R., 2000. Precise temporal correlation of holocene mollusk shells using sclerochronology. Quaternary Research 53, 236–246.
Martinez, E., Antoine, D., D'Ortenzio, F., Gentilli, B., 2009. Climate-driven basin-scale decadal oscillations of oceanic phytoplankton. Science 326, 1253–1256.
Meng, X., 1994. Posterior predictive *p*-values. Annals of Statistics 22, 1142–1160.
Minte-Vera, C.V., Branch, T.A., Stewart, I.J., Dorn, M.W., 2005. Practical application of meta-analysis results: avoiding the double use of data. Canadian Journal of Fisheries and Aquatic Sciences 62, 925–929.
Noakes, D.J., Campbell, A., 1992. Use of geoduck clams to indicate changes in the marine environment of Ladysmith Harbor, British-Columbia. Environmetrics 3, 81–97.
Pilling, G.M., Kirkwood, G.P., Walker, S.G., 2002. An improved method for estimating individual growth variability in fish, and the correlation between von Bertalanffy growth parameters. Canadian Journal of Fisheries and Aquatic Sciences 59, 424–432.
Punt, A.E., Hilborn, R., 1997. Fisheries stock assessment and decision analysis: the Bayesian approach. Review of Fisheries Biology and Fish 7, 3563.
Ricker, W.E., 1975. Computation and interpretation of biological statistics of fish populations. Bulletin of the Fisheries Research Board of Canada, No. 191.
Shaul, W., Goodwin, L., 1982. Geoduck (*Panope generosa*: Bivalvia) age as determined by internal growth lines in the shell. Canadian Journal of Fisheries and Aquatic Sciences 39, 632–636.
Smith, A., Wakefield, J.C., 1994. The hierarchical Bayesian approach to population pharmokinetic modeling. International Journal of Bio-medical Computing 36, 35–42.
Speer, J.H., 2010. Fundamental of Tree-Ring Research. University of Arizona Press, Tucson, AZ.
Spiegelhalter, D., 2006. Some DIC Slides. IceBUGS, Finland, 11–12 February 2006. Available at: http://www.mrc-bsu.cam.ac.uk/bugs/winbugs/DIC-slides.pdf
Spiegelhalter, D.J., Best, N.G., Carlin, B.P., Van der Linde, A., 2002. Bayesian Measures of Model Complexity and Fit (with Discussion). Journal of the Royal Statistical Society, Series B 64, 583–616.
Spiegelhalter, D., Thomas, A., Best, N., Lunn, D., 2003. WinBUGS User Manual, Version 1.4. Available at: http://www.mrc-bsu.cam.ac.uk/bugs
Stokes, M.A., Smiley, T.L., 1996. An Introduction to Tree-ring Dating. University of Arizona Press, Tucson, AZ.
Strom, A., Francis, R.C., Mantua, N.J., Miles, E.L., Peterson, D.L., 2004. North Pacific climate recorded in growth rings of geoduck clams: a new tool for paleoenvironmental reconstruction. Geophysical Research Letters, 31.
Von Rosen, D., 1997. On moments of the inverted Wishart distribution. Statistics 30, 259–278.
Wade, P.R., 2000. Bayesian methods in conservation biology. Conservation Biology 14, 1308–1316.
Weisberg, S., 1993. Using hard-part increment data to estimate age and environmental effects. Canadian Journal of Fisheries and Aquatic Sciences 50, 1229–1237.
Weisberg, S., Spangler, G., Richmond, L.S., 2010. Mixed effects models for fish growth. Canadian Journal of Fisheries and Aquatic Sciences 67, 269–277.
Whitney, R., Carlander, K.D., 1956. Interpretation of the body-scale regression of computing body length of fish. Journal of Wildlife Management 20, 21–27.
Zeger, S.L., Liang, K.Y., 1986. Longitudinal data analysis for discrete and continuous outcomes. Biometrics 42, 121–130.